1.5 μm, 8 × 12.5 Gb/s of hybrid-integrated TOSA with isolators and ROSA for 100 GbE application

Zeping Zhao (赵泽平)[1], Yu Liu (刘 宇)[1,*], Zhike Zhang (张志珂)[1], Xiangfei Chen (陈向飞)[2], Jianguo Liu (刘建国)[1], and Ninghua Zhu (祝宁华)[1]

[1]*State Key Laboratory on Integrated Optoelectronics, Institute of Semiconductors, Chinese Academy of Sciences, Beijing 100083, China*
[2]*Microwave-Photonics Technique Laboratory National Laboratory of Microstructures & School of Engineering and Applied Sciences, Nanjing University, Nanjing 210093, China*
*Corresponding author: yliu@semi.ac.cn

Compact transmitter and receiver optical sub-assemblies (TOSA and ROSA) are fabricated in our laboratory and have an aggregated capacity of 100 Gb/s. Specially, directly modulated laser (DML) drivers with two layers of electrical circuit boards are designed to inject RF signals and bias currents separately. For all the lanes, the 3 dB bandwidth of the cascade of the TOSA and ROSA exceeds 9 GHz, which allows the 12.5 Gb/s operation. With the 12.5 Gb/s × 8-lane operation, clear eye diagrams for back-to-back and 30-km amplified transmission with a dispersion compensation fiber are achieved. Low cost and simple processing technology make it possible to realize commercial production.

OCIS codes: 060.0060, 140.0140, 230.0230, 250.0250.
doi: 10.3788/COL201614.120603.

With the increasing demand for huge data capacity for communication systems, optical transceivers play an significant role in achieving high bit rates, low power consumption, and compact package sizes. To meet the demand, 100 Gbit Ethernet (100 GbE) was standardized in 2010[1]. High single-channel data rates and wavelength-division multiplexing are two ways to realize a high transmission capacity[2,3]. However, the bit rate of the laser is limited and the package for a high-frequency laser chip suffers from many difficulties, especially in the design of a microwave circuit. Therefore, using multi-lane approaches, such as coarse wavelength-division multiplexing (CWDM), is a good way to realize large capacities.

Much research work has been done to keep up with the 100 GbE standard. Electro-absorption modulated distributed feedback (EADFB) laser array chips are used to achieve high-capacity multi-wavelength networks[4]. However, the main problem with using an EADFB laser array is the high power consumption. Compared with externally modulated lasers (EMLs), directly modulated lasers (DMLs) have many advantages, such as low power consumption, small size, and low cost. Due to these merits, DMLs are widely used as optical source[5–7]. It is worth noting that the manufacture of monolithic integrated multi-wavelength laser arrays has a high cost and low production yield, whether it is for EMLs or for DML array chips. What is more, the wavelengths of laser array chips are not easily controlled.

For 100 GbE transceiver construction, compact size is also important point that should be taken into consideration. Generally, in order to get a compact optical transceiver, different integration schemes have been adopted. Monolithic integration can effectively reduce the module size, but it has a high requirement for technology[8]. For multiple-lane transmitters, the requirement for wavelengths is extremely rigid; for a monolithic integrated laser chip, if any of channels have an existing wavelength shift, the chip will be unavailable. Therefore, the main weaknesses for monolithic integration are high cost and low number of finished products. To alleviate this situation, hybrid integration has been proposed. Hybrid integration, in which individual functional components are fabricated in different materials and combined on a common substrate, is a feasible path to realize high production. Moreover, we can test individual components prior to assembly and select the appropriate wavelength independently.

Various multi-lane configurations with hybrid integration for 100 GbE applications have been reported[9–11]. However, for most of them, optical isolators have been "missing" components in photonic circuits, even though optical isolators play important roles in ensuring the stable operation of LDs. The performances, such as the output power, spectrum, relative intensity noise (RIN), dispersion penalty, and bit error rate (BER) of the transmitter optical sub-assembly (TOSA), are optimized by reducing the optical reflection[12,13].

In this Letter, a hybrid-integrated transmitter module with eight independent optical isolators is assembled. Therefore, light reflection can be effectively prevented from feeding back into the distributed feedback (DFB) laser and the adiabatic chirp also will be suppressed[14]. The TOSA and receiver optical sub-assembly (ROSA) we developed can provide an aggregate capacity of 100 Gb/s distributed over 8 channels on a 200 GHz frequency grid. They not only can be used for eight independent
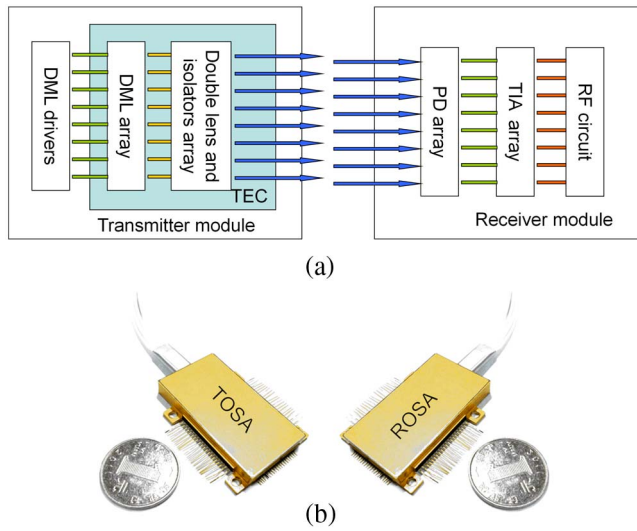
(a)

(b)

Fig. 1. (a) Schematic arrangement of the hybrid-integrated TOSA and ROSA module. (b) Photograph of the TOSA and ROSA.

transmission systems with different directions, which helps to simplify communication systems and save space, but they can also be used as integrated modules to realize DWDM transmission.

As shown in Fig. 1(a), the transmitter module comprises three parts: a ceramic board with laser drivers, eight independent laser chips array with 2 mm pitch, and isolators and a double-lens array along with eight independent optical fibers for light coupling. For an 8-laser-chip array, an InGaAsAl multiple quantum well (MQW) is used as the active region, and the chips are fabricated by conventional two-stage lower-pressure metal-organic vapor phase epitaxy (MOVPE). The wavelength of the 1.5 µm DFB laser is well controlled with a fine grating structure, such as phase shifts based on the reconstruction-equivalent-chirp (REC) technique[15,16]. The DML array, double lens, and isolator array share a common thermoelectric cooler (TEC) for thermal stabilization.

The receiver module also consists of three portions, as shown in Fig. 1(a): an eight-PIN-chip array with a 2 mm interval, a TIA array, and an RF circuit board. Both the transmitter module and receiver module are packaged in butterfly housing, as shown in Fig. 1(b), in which DC pins with a 2.54 mm pitch are placed on two sides to provide a bias current for the lasers or bias voltage for the detectors. The high-frequency pins that are arranged at the front end of the body are specially designed to input or output the frequency signal.

Microwave circuit design is very important to obtain a good performance for TOSA. For the RF circuit board design, electrical crosstalk, which seriously deteriorates the transmission performance, should be mainly considered, so we propose two methods to suppress the electrical crosstalk in the TOSA.

One of the technical keys is achieving the side metallization of transmission lines whose structure is coplanar
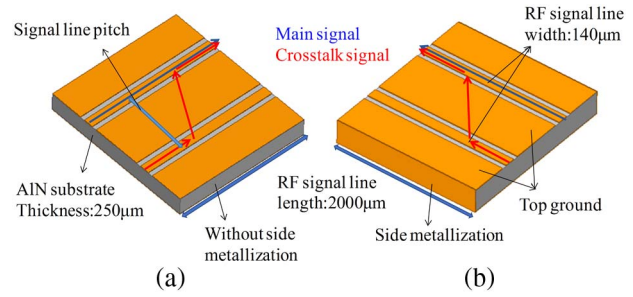

Fig. 2. Simulation model of the RF circuit board. (a) CPW without side metallization. (b) CPW with side metallization.

waveguide (CPW) side metallization. With this method, the ground electrodes of the top surface and bottom surface are connected together; thus, great grounding effect is achieved and the electromagnetic field of the microwave signal can be effectively constrained. Figure 2 shows the simulation model of the RF circuit. In order to match with the 50 Ω system, the characteristic impedance of the CPW transmission lines should be designed to be 50 Ω to reduce electrical reflections. This can be determined as follows[17,18]:

$$Z_0 = \frac{60\pi}{\sqrt{2(\varepsilon_r + 1)}RoE(K)}, \tag{1}$$

$$K = \frac{1}{1 + 2\frac{L}{W}}. \tag{2}$$

where W and L are the width of the signal line and the gap between the signal line and the ground line, respectively. ε_r is the relative dielectric constant of the substrate material. Based on this equation, we set the signal width W and gap L at 140 and 70 µm, respectively. The signal line pitch is 1000 µm, and the AlN substrate is 250 µm thick with a relative permittivity of 8.7. Figure 3 shows the simulation results of the electrical crosstalk. The results show that the electrical crosstalk with side metallization is decreased compared with that without metallization. Even though the electrical crosstalk is only decreased by 1 dB, the method of side metallization has
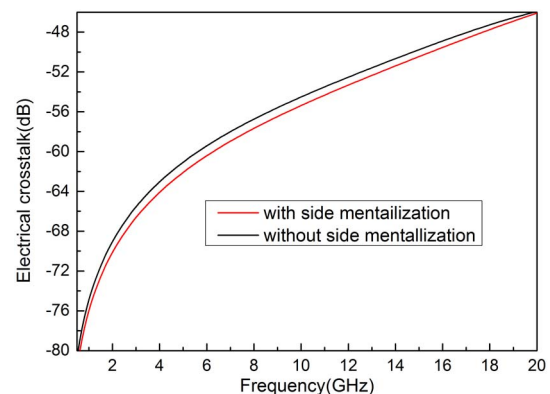

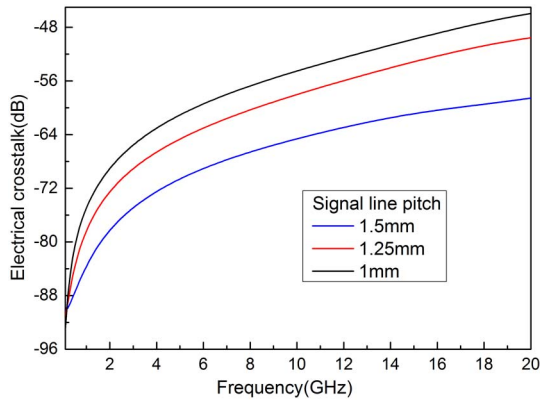Fig. 3. Electrical crosstalk of the RF circuit board.

Fig. 4. Signal lines' pitch dependence on electrical crosstalk.

indeed contributed to reducing the electrical crosstalk. What is more, it helps to guarantee the signal integrity.

The other technical key is widening the width of the pitch between the RF signal lines. The simulation model can be seen in Fig. 2(a). Figure 4 shows the simulation results of the width between the RF signal lines dependent on the electrical crosstalk. The results show that the electrical crosstalk is decreased as the signal line pitch increases. However, the width of the circuit board is limited, and if many DC lines and eight RF lines are all installed at the rear end of an optical transmitter package, the electrical crosstalk will be increased due to the small pitch of the RF signal lines. To solve this problem, we have proposed a simple and effective scheme in which the circuit board has two layers, as shown in Fig. 5. The signal lines and DC lines are placed on two different inner circuit boards, and then the two circuit boards are stacked in the package. In this way, the pitch of the RF signal line can be widened so as to reduce the crosstalk. In addition, we can inject RF signals and bias currents separately and make the working current more easily controlled. The termination resistances (red area) on the signal line end are set to 45 Ω to realize 50-Ω independence matching. Because the currents directly transfer on top of the circuit board and do not pass the 45-Ω resistors, it helps to reduce the generation of heat, which effectively decreases the power consumption. The inductors are fabricated on the top layer to
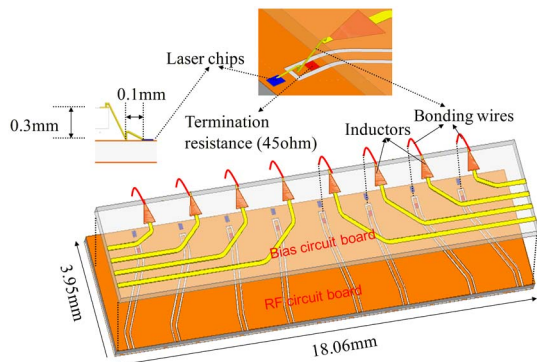
prevent RF signals. Inductors here should have a good high-frequency property: the better the high-frequency property, the more effective the inductor is at preventing RF signals. The DC lines connect with RF lines through a bonding wire which is made of gold and has a diameter of 25 μm. The laser chips are placed on the end of the RF circuit board (blue area). RF signals are fed into the laser chips through the bonding wires. Because bonding wires have parasitic inductances that degrade the high-frequency bandwidth, the bonding wires between the laser chip and the RF signal line should be as short as possible. The pitch of the signal line is 2 mm, which is same as that of the laser chip. It can be estimated that the crosstalk of the RF signal lines is lower than that of the 1.5 mm pitch.

In all the measurements for the transmitter module, the chip temperature is set at 25°C. Figure 6 shows the *P-I* characteristic of the eight lanes. The maximum output optical power of the chips used for packaging is about 10 mw, and the coupling efficiency is ~50% by using a double lens and the isolator coupling method. The optical power of all the lanes is around 5 mW with a bias current of 40 mA, as shown in Fig. 6. The threshold current of each lane is approximately 10 mA. The results show that the threshold currents are nearly independent of the wavelengths. Figure 7 shows the E/O response of the cascade of the
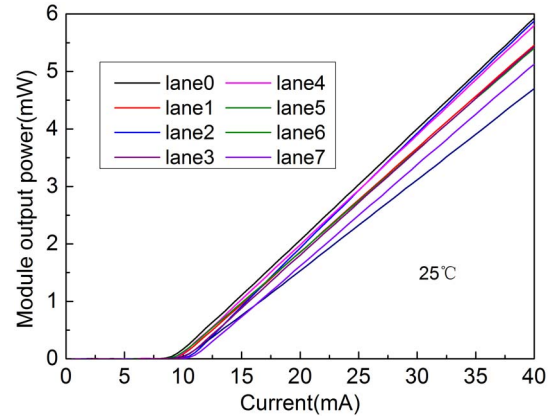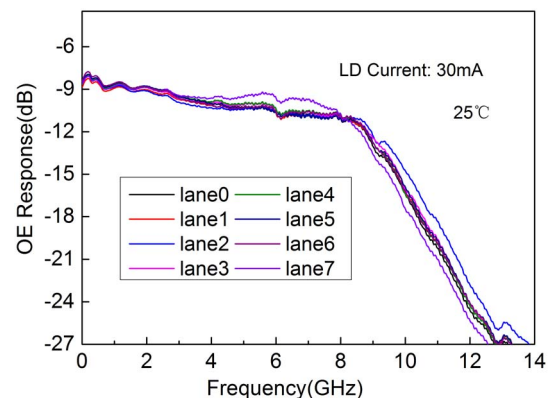

Fig. 6. *P-I* characteristic of TOSA.

Fig. 5. Schematic structure of the two-layer circuit board.

Fig. 7. E/O response of the cascade of TOSA and ROSA.
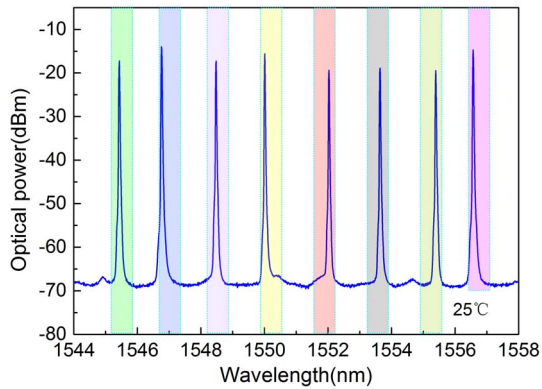
Fig. 8. Lasing spectrum of DML array (colored areas indicate LAN-WDM grid).

Fig. 9. Schematic test setup. PPG: pattern generator. BERT: bit error-rate tester.

transmitter module and the receiver module. For all lanes, the 3 dB bandwidths exceed 9 GHz when the LD currents are set at 30 mA, which allows the 12.5 Gb/s operation.

Finally, we measured the transmission characteristics for the TOSA and ROSA. Figure 8 shows the lasing spectrum of the TOSA, which is obtained through operating eight lanes simultaneously with a bias current of 30 mA for all channels. In order to measure eight channel wavelengths at the same time, a planar lightwave circuit (PLC) optical power combiner, whose insertion loss is about equal to 10 dB, has been used. That is the main reason for the low optical power in Fig. 8. The side-mode suppression ratios (SMSRs) exceed 45 dB. The results also show that the device exhibits a clear side-mode operation for all the channels. The eight peak wavelengths are 1545.43, 1546.76, 1548.48, 1550.01, 1552.03, 1553.64, 1555.26, and 1556.57 nm, which accord with the standard ITU-T recommendation, as indicated in Fig. 8. The adjacent channel spacing is about 200 GHz. Both the carrier and thermal have an effect on the wavelength tuning mechanism. Because all the laser chips share a common TEC, the changes of the currents with different channels will vary the temperature gradient within the laser chip. Therefore, the wavelength of one channel is also determined by the currents of the other channels. We found the relation of the wavelengths of the laser chip array and the injection currents of all the lanes is approximately linear, so the uniformity of the optical spectrum is improved by adjusting the injection current based on this relationship.

The transmission over amplified links performance is assessed with the experimental setup schematically shown in Fig. 9. DC-bias currents of 30 mA with peak-to-peak swings of 0.5–0.7 Vpp are applied to the TOSA's DMLs, and all lasers are driven by 12.5 Gb/s, non-return-to-zero (NRZ), PBRS $2^{31}-1$ signals supplied by pulse pattern generators. AWGs are used as the multiplexer (MUX) and demultiplexer (DEMUX). The spacing of adjacent lanes for the AWGs is 50 GHz, and we chose the corresponding channel for transmission. The signals are launched into a single-mode fiber that is 20 km long. For a directly modulated mode DFB at 1550 nm transmission, we expect a serious dispersion, so a 10 km dispersion
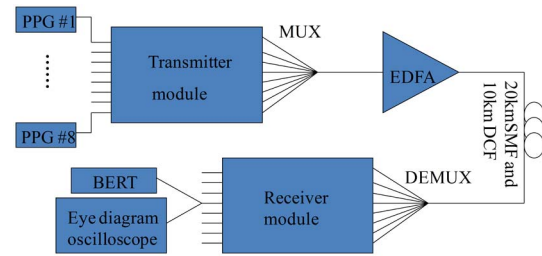
compensation fiber is used to improve this situation. For links of 30 km, we use an erbium-doped fiber amplifier (EDFA) in the middle of the link to compensate for link losses. Finally, the light passes through the demultiplexer before being fed into the ROSA for detection.

Table 1 shows clear eye diagrams for back-to-back (B-to-B) configurations. All eight channels are operated at 12.5 Gb/s, and clear eye openings without any distortion-like overshoots and ripples are obtained. After 30-km transmission, we also obtain clear eye diagrams for all eight lanes, as shown in Table 2. We can see the upper eyelids of the eye diagram are coarsened, most likely due to an impedance mismatch in the system. Dispersion and attenuation effects in optical fiber will seriously deteriorate the signal quality, causing rising and falling edges to bolded and multiple paths to appear for long-distance transmissions. For 30-km transmissions, the dynamic extinction ratios (DERs) of lanes 0, 1, 2, 3, 4, 5, 6, and 7 are 5.0, 5.2, 5.6, 5.4, 5.1, 5.0, 5.2, and 5.3 dB, respectively.

These results indicate that the 8-channel hybrid-integrated TOSA and ROSA can be applied to 100 GbE transmission, and it is possible to realize commercial

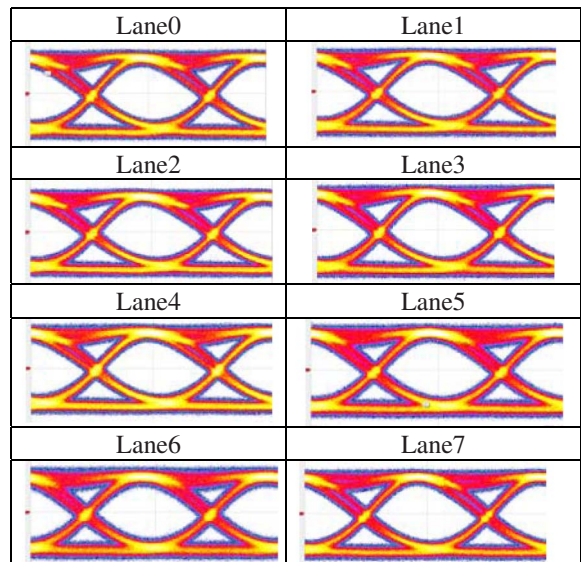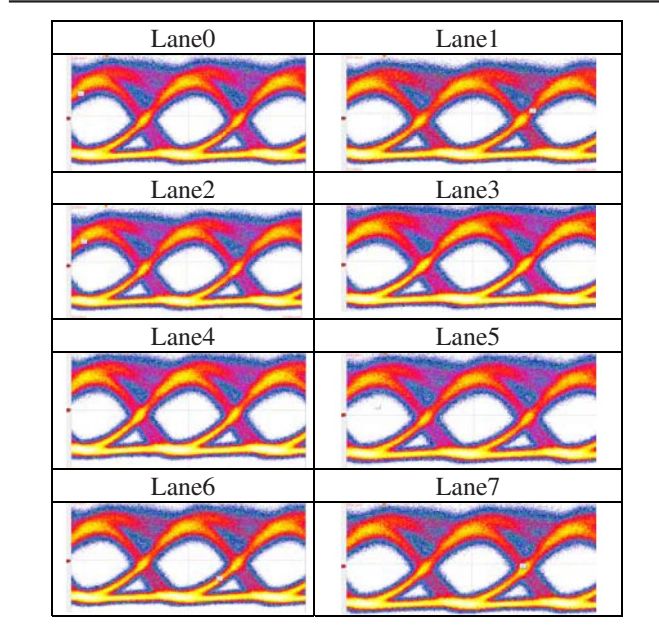**Table 1.** Eye Diagrams Under 100 Gb/s Operation for B-to-B

Lane0	Lane1
Lane2	Lane3
Lane4	Lane5
Lane6	Lane7

Table 2. Eye Diagrams Under 100 Gb/s Operation for 30-km Transmission

Lane0	Lane1
Lane2	Lane3
Lane4	Lane5
Lane6	Lane7

production due to the advantages of low cost and simple processing technology.

References

1. C. Cole, "Beyond 100G client optics," http://www.ieee802.org/3/ba/ (2012).
2. Z. Zhang, X. Jiang, J. Wang, X. Chen, and L. Wang, Chin. Opt. Lett. **13**, 020603 (2015).
3. B. Pezeshki, J. Heanue, D. Ton, T. Schrans, S. Rangarajan, S. Zou, G. W. Yoffe, A. Liu, M. Sherback, J. Kubicky, and P. Ludwig, J. Lightwave Technol. **32**, 2796 (2014).
4. S. Hurt, A. G. Dentai, J. L. Pleumeekers, and A. Mathur, in *Proceeding of IEEE Conference on Device Research*, 183 (2007).
5. W. Kobayashi, T. Tadokoro, T. Ito, T. Fujisawa, T. Yamanaka, Y. Shibata, and M. Kohtoku, in *Proceeding of IEEE Conference on International Semiconductor Laser*, 50 (2012).
6. T. Simoyama, M. Matsuda, S. Okumura, A. Uetake, M. Ekawa, and T. Yamamoto, in *Proceeding of IEEE Conference on International Semiconductor Laser*, 54 (2012).
7. W. Kobayashi, T. Fujisawa, K. Tsuzuki, Y. Ohiso, T. Ito, S. Kanazawa, T. Yamanaka, and H. Sanjoh, J. Lightwave Technol. **32**, 3 (2014).
8. J. Zhao, X. Chen, N. Zhou, X. Huang, and W. Liu, Chin. Opt. Lett. **12**, 99 (2014).
9. T. Schrans, G. Yoffe, Y. Luo, and R. Narayan, in *Proceeding of IEEE Conference on Optical fiber Communication*, 1 (2009).
10. J. Wang, Y. Liu, X. Chen, J. Liu, and N. Zhu, Chin. Sci. Bull. **59**, 2387 (2014).
11. P. Bernasconi, L. Buhl, D. T. Neilson, J. H. Sinsky, N. Basavanhally, C. Bolle, M. A. Cappuzzo, E. Y. Chen, M. Earnshaw, R. Farah, R. Frahm, A. Gasparyan, D. Gill, L. Gomez, R. Keller, F. Klemens, P. Kolodner, Y. Low, R. Papazian, F. Pardo, D. Ramsey, M. S. Rasras, T. Salamon, E. M. Simon, E. Sutter, M. Achouche, S. Barbet, F. Blanche, F. Brillouet, N. Chimot, J. Decobert, H. Debregeas, O. Drisse, F. Franchin, H. Gariah, J.-L. Gentner, G. Glastre, N. Lagay, D. Lanteri, F. Lelarge, F. Mallecot, F. Pommereau, J.-G. Provost, G. Azzini, L. Fratta, P. Galli, V. Guja, S. Jovane, D. Palmisano, F. Perego, and R. Peruta, IEEE Photon. Technol. Lett. **24**, 1657 (2012).
12. Y. Huang, T. Okuda, K. Sato, Y. Muroya, T. Sasaki, and K. Kobayashi, IEEE Photon. Technol. Lett. **13**, 245 (2001).
13. R. T. Sahara, R. A. Salvatore, A. Hohl-Abichedid, and H. Lu, IEEE J. Quantum Electron. **38**, 620 (2002).
14. J. Zhang, N. C. Frateschi, W. Choi, H. Gebretsadik, R. Jambunathan, and A. E. Bond, Electron. Lett. **39**, 1841 (2003).
15. Y. Ni, X. Kong, X. Gu, G. Zheng, and J. Luan, Chin. Opt. Lett. **312**, 37 (2013).
16. J. Hou, X. Chen, L. Wang, W. Chen, and N. Zhu, IEEE Photon. J. **4**, 2189 (2012).
17. Z. Zhang, Y. Liu, J. Wang, J. Bai, H. Yuan, X. Wang, J. Liu, and N. Zhu, IEEE Photon. J. **8**, 1 (2016).
18. Z. K. Zhang, Y. Liu, J. G. Liu, and N. H. Zhu, J. Semicond. **36**, 3 (2015).